Heterogeneous Catalysis

International Edition: DOI: 10.1002/anie.201508128
German Edition: DOI: 10.1002/ange.201508128

Identifying Different Types of Catalysts for CO_2 Reduction by Ethane through Dry Reforming and Oxidative Dehydrogenation

*Marc D. Porosoff, Myat Noe Zin Myint, Shyam Kattel, Zhenhua Xie, Elaine Gomez, Ping Liu, and Jingguang G. Chen**

Abstract: *The recent shale gas boom combined with the requirement to reduce atmospheric CO_2 have created an opportunity for using both raw materials (shale gas and CO_2) in a single process. Shale gas is primarily made up of methane, but ethane comprises about 10% and reserves are underutilized. Two routes have been investigated by combining ethane decomposition with CO_2 reduction to produce products of higher value. The first reaction is ethane dry reforming which produces synthesis gas ($CO + H_2$). The second route is oxidative dehydrogenation which produces ethylene using CO_2 as a soft oxidant. The results of this study indicate that the Pt/CeO_2 catalyst shows promise for the production of synthesis gas, while Mo_2C-based materials preserve the C–C bond of ethane to produce ethylene. These findings are supported by density functional theory (DFT) calculations and X-ray absorption near-edge spectroscopy (XANES) characterization of the catalysts under in situ reaction conditions.*

Recent exploitation of shale gas reserves has increased the importance of using methane and the heavier gas fractions as raw materials for producing chemicals and fuels. Methane is the primary component of shale gas, but ethane comprises approximately 10%, with the exact concentration depending on the particular source.[1] Most ethane is converted by thermal dehydrogenation into ethylene, a valuable commodity chemical, at high temperatures, between 750–950°C, in the presence of steam,[2] which is energy-intensive and leads to coke formation on the reactor walls and catalyst bed.[3] Catalysts that can effectively convert ethane to useful products at lower temperatures, without coke formation, are very desirable. Ideally, a catalyst that can use CO_2 as the oxidant is particularly useful because the reduction of CO_2 can help mitigate ocean acidification and climate change,[4] while unreacted CO_2 can also reduce coke formation through the reverse Boudouard reaction ($CO_2 + C \rightarrow 2CO$), which has been shown to occur as low as 500°C,[5] thus increasing conversion and catalyst stability.[3]

CO_2 reduction by ethane can proceed through two distinct pathways: 1) reforming to produce synthesis gas ($2CO_2 + C_2H_6 \rightarrow 4CO + 3H_2$) and 2) oxidative dehydrogenation (ODH) to produce ethylene ($CO_2 + C_2H_6 \rightarrow C_2H_4 + CO + H_2O$). For decades, researchers have attempted dry reforming of methane and CO_2, but breakthroughs have been difficult because of the high reaction temperatures (ca. 700°C) and deactivation of catalysts.[6] Dry reforming of ethane, however, becomes thermodynamically favorable at a lower temperature than for methane (ca. 600°C), making the process more feasible under milder conditions.[7] The difference in reaction temperatures between ethane and methane dry reforming also provides a potential opportunity for reactively separating shale gas, thereby directly producing synthesis gas from ethane and CO_2, while leaving the methane unreacted.

ODH of ethane by CO_2 is another important pathway because of the high energy requirement for the current ethane dehydrogenation processes.[8] Several groups have studied ODH of ethane with pure O_2,[9] which is more reactive but does not have the added benefit of reducing CO_2 emissions. ODH of ethane with CO_2 as a mild oxidant is proposed to occur through a Mars-van-Krevelen-type mechanism,[10] where the catalyst first dehydrogenates ethane into ethylene and H_2, then H_2 reduces CO_2 to CO through the reverse water-gas shift (RWGS) reaction, producing H_2O as a byproduct.[11] At 600°C, both the reforming and ODH reactions occur simultaneously, thus it is necessary to identify classes of catalysts to kinetically control the extent of reforming versus ODH. It is highly desirable to identify distinct types of catalysts that can 1) efficiently break the C–C bond to produce synthesis gas, or 2) selectively break C–H bonds of ethane while preserving the C–C bond to produce ethylene.

Previous research indicates that typical catalysts used for CO_2 reduction by ethane are Cr-based oxide catalysts. Cr_2O_3 catalysts convert high amounts of ethane, but overall CO_2 conversion is low with short lifetimes, likely because of coke formation.[12] There is a support effect, with SiO_2 displaying the highest activity,[13] and doping the catalyst with small amounts of Fe, Co, and Mn further improves ethylene selectivity.[14] The high activity of Cr-based catalysts could stem from their ability to exist in several oxidation states, similar to Mn-based molecular sieve catalysts.[12] Ga_2O_5 and Ca-doped ThO_2 are reducible materials that are also active and selective for this reaction,[15] while a nanostructured CeO_2 catalyst doped with CaO oxidizes ethane into CO and H_2O, with ODH as the side reaction. For carbide catalysts, Mo_2C/SiO_2 has about 10% conversion with high ethylene selectiv-

[*] Dr. M. D. Porosoff, Z. Xie, E. Gomez, Prof. Dr. J. G. Chen
Department of Chemical Engineering, Columbia University
500 W. 120th St., New York, NY 10027 (USA)
E-mail: jgchen@columbia.edu
M. N. Z. Myint
Department of Chemical and Biomolecular Engineering
University of Delaware, 150 Academy St.
Newark, DE 19716 (USA)
Dr. S. Kattel, Dr. P. Liu, Prof. Dr. J. G. Chen
Chemistry Department, Brookhaven National Laboratory
2 Center St., Upton, NY 11973 (USA)

Supporting information for this article is available on the WWW under http://dx.doi.org/10.1002/anie.201508128.

ity; however, pure Mo_2C and MoO_3/SiO_2 are not reported as active.[16]

Although there have been studies into CO_2 reduction by ethane, details are lacking on how to control the extent of dry reforming versus ODH. In the current study, two types of catalysts, metals (Pt-based) and metal carbides (Mo_2C), are investigated under identical reaction conditions to differentiate the two reaction pathways. It is hypothesized that Pt and Mo_2C-based systems are promising catalysts to study reforming and ODH during CO_2 reduction by ethane because Pt catalysts supported on CeO_2[17] and Mo_2C[18] are both active for RWGS from their high oxygen mobility, a critical feature required for CO_2 reduction by ethane. The findings of this study confirm that although there is deactivation, Pt/CeO_2 favors the reforming reaction and Mo_2C-based catalysts are more selective at producing the ODH product, ethylene. These novel findings are supported by DFT calculations and in situ X-ray absorption near-edge spectroscopy (XANES) measurements.

To help identify reaction pathways over the two types of catalysts, density functional theory (DFT) calculations were performed to compare differences in binding energies of potential reaction intermediates. The results in Table 1 show that all intermediates bind more strongly on $Mo_2C(001)$ than on Pt(111). It is noted that, for adsorbates with similar binding configurations, the binding energy difference between Pt(111) and $Mo_2C(001)$ is more pronounced for species adsorbed by the oxygen atom than those using the carbon atom. This is due to the much higher affinity of the $Mo_2C(001)$ surface toward O relative to Pt(111). The DFT calculated BE_{diff} is 3.53 eV for atomic oxygen, while it is only 1.60 eV for atomic carbon.

Table 1: DFT-calculated binding energies (in eV) of ethane dehydrogenation intermediates and atomic O and C on Pt(111), $Ce_3O_6/Pt(111)$, and $Mo_2C(001)$ surfaces.

Species	Pt(111)	Ce_3O_6/Pt(111)	$Mo_2C(001)$	$BE_{diff} = BE_{Pt(111)} - BE_{Mo2C(001)}$
CH_3CH_2O	−1.62	−2.42	−4.22	2.60
CH_3CHO	−0.31	−0.95	−2.30	1.99
CH_3CO	−2.36	−2.99	−3.81	1.45
CH_3CH_2	−1.97	−1.97	−2.98	1.01
CH_2CH_2	−1.09	−1.24	−2.23	1.14
CH_2CH	−3.18	−3.42	−4.64	1.46
CH_3	−2.11	−2.26	−3.14	1.03
CO	−1.76	−2.19	−2.72	0.96
H	−2.75	−2.80	−3.37	0.62
O	−4.11	−4.33	−7.64	3.53
C	−7.17	−5.55	−8.77	1.60

DFT was also used to calculate the enthalpy change for the oxidative C–C and C–H bond cleavage of ethane on Pt(111) and $Mo_2C(001)$ surfaces. The C–C bond cleavage of ethane produces CH_3*, CO*, and $H_2O(g)$, while C–H bond scission results in the formation of CH_2CH_2* and $H_2(g)$. For the case of Pt(111) in Figure 1a, atomic hydrogen is assumed to form $H_2O(g)$ since both OH ($O^* + H^* \rightarrow OH^*$) and H_2O formation ($H^* + OH^* \rightarrow H_2O^*$) are exothermic processes on the Pt(111) surface.[19] This is not the case, however, for

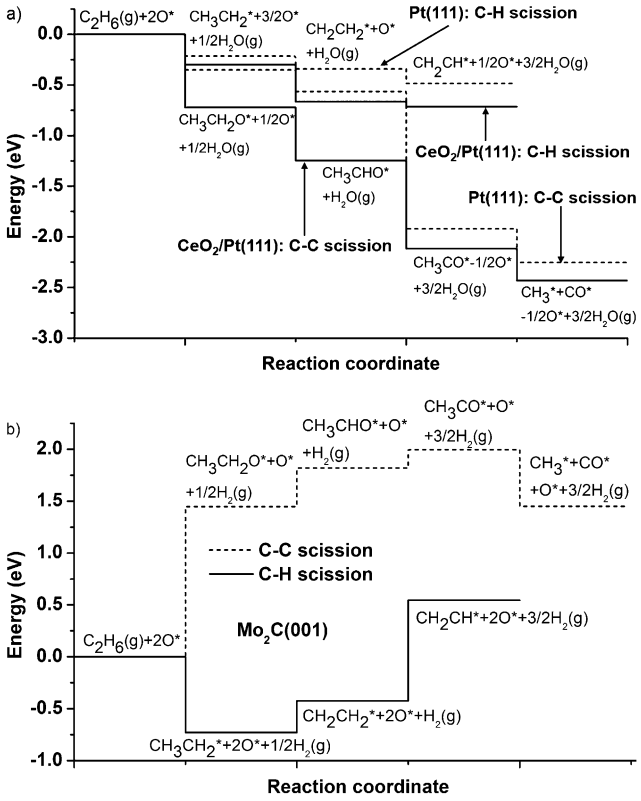

Figure 1. DFT-calculated energy profile of reforming and oxidative dehydrogenation of ethane on a) Pt(111) and CeO_2/Pt(111) and b) the $Mo_2C(001)$ surface.

$Mo_2C(001)$ in Figure 1b, where both OH ($O^* + H^* \rightarrow OH^*$) and H_2O formation ($H^* + OH^* \rightarrow H_2O^*$) are highly endothermic processes.[20] Over $Mo_2C(001)$, the atomic hydrogen prefers to recombine and desorb from the surface in the form of hydrogen gas.

Furthermore, Figure 1a shows that on Pt(111), the C–C bond cleavage of ethane to form CH_3*, CO*, and $H_2O(g)$ is not only exothermic, but also more favorable compared to the selective C–H bond cleavage to form CH_2CH_2*. More specifically, oxidation of ethane to form CH_3CH_2O* is energetically more favorable than the dehydrogenation of ethane to form CH_3CH_2* in the presence of oxygen on the surface. On Pt(111), CH_3CH_2O* undergoes two successive dehydrogenation reactions to form CH_3CO*, which then undergoes C–C bond cleavage to form CH_3* and CO*. Thus, the Pt(111) surface promotes reforming of ethane to form CO.

A different reaction scheme from that on Pt(111) is observed on $Mo_2C(001)$. The stronger affinity of $Mo_2C(001)$ for oxygen makes C–O bond formation less favorable on $Mo_2C(001)$ than on Pt(111), which agrees well with previous studies showing that $Mo_2C(001)$ binds carbon and oxygen very strongly, leading to spontaneous cleavage of the C–O bond.[21] Therefore, as shown in Figure 1b, the $Mo_2C(001)$ surface preferentially dehydrogenates ethane to form CH_2CH_2*. Further discussion of the possible origins of the selective adsorption of different intermediate species over Pt(111) and $Mo_2C(001)$ is provided in the Supporting Information.

Further DFT calculations were performed on CeO_2/Pt(111) to investigate the role of the Pt–CeO_2 interface in the energy profile of reforming and oxidative dehydrogenation of ethane. The O-containing species bind at the Pt–CeO_2 interface and most of the hydrocarbon species bind at the Pt sites, with detailed figures available in the Supporting Information. More importantly, the calculated energy profile for the reforming of ethane on CeO_2/Pt(111) and Pt(111) in Figure 1 shows a similar trend; however, the reaction is more thermodynamically favorable on CeO_2/Pt(111), which is associated with the strong CeO_2–Pt(111) interaction[22] and therefore strengthened binding of O-containing species at the interface, as shown in Table 1. Thus, the DFT results suggest that similar to Pt(111), CeO_2/Pt(111) also enhances the reforming of ethane.

To verify the DFT predictions, reactions of ethane and CO_2 were evaluated in a quartz reactor under atmospheric pressure. The activity and selectivity as a function of time on stream for the catalysts, Pt/CeO_2 and Mo_2C/γ-Al_2O_3, are compared in Figure 2. Furthermore, alloying Co with the Pt/CeO_2 catalyst improves the catalytic stability. The comparison between the two catalysts clearly reveals differences in performance. Pt/CeO_2 shows higher activity and selectivity toward reforming products, but Mo_2C/γ-Al_2O_3 has a lower activity with increased ethylene selectivity, confirming the trend seen in the DFT calculations.

The difference in activity between the two classes of catalysts can be further explained through measuring the apparent activation barrier of both CO_2 and ethane over Pt/CeO_2 and Mo_2C/γ-Al_2O_3, as shown in Figure 3. Over Pt/CeO_2 the activation barriers are 16.0 kcal mol^{-1} and 21.6 kcal mol^{-1} for CO_2 and ethane, respectively, and on Mo_2C/γ-Al_2O_3 the values are 19.5 kcal mol^{-1} and 17.5 kcal mol^{-1}. The lower activation barrier of CO_2 over Pt/CeO_2 confirms the relatively high activity of CeO_2-based materials toward CO_2.[23]

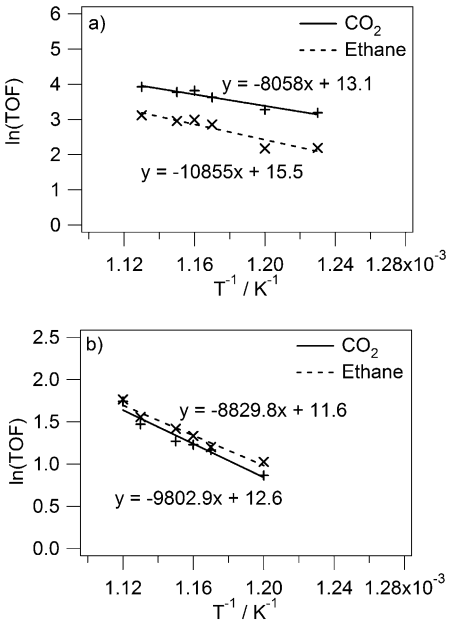

Figure 3. Activation barrier plots represented as ln(TOF) versus 1/*T* for a) Pt/CeO_2 and b) Mo_2C/γ-Al_2O_3 at six temperatures. Values of TOF calculated by averaging data points between 2–4.5 h on stream.

Because CeO_2 has been shown to be an excellent support for reactions involving CO_2, an additional test was performed by supporting Mo_2C on CeO_2. As seen in Table 2, comparisons of conversion indicate there is a clear support effect for Mo_2C, where γ-Al_2O_3 slightly improves the activity over the pure carbide, but CeO_2 appears to diminish the activity. This support effect likely suggests that the greater acidity of γ-Al_2O_3 promotes the binding of ethane, which is consistent with previous work indicating that oxidative dehydrogenation of alkanes is strongly dependent on the acidity of support materials.[24] However, future studies will be required to determine the effect of acidity on the reaction pathways of CO_2 and ethane over Mo_2C/γ-Al_2O_3.

Furthermore, the behavior of Mo_2C/γ-Al_2O_3 is more similar to that of pure Mo_2C than Mo_2C/CeO_2, which is likely from the low surface area and CO uptake of Mo_2C/CeO_2 (0.8 μmol g^{-1}). It is also possible that the high intrinsic activity of both CeO_2 and Mo_2C[21b] towards CO_2 bond scission creates an excess of adsorbed O on the catalyst surface, which quickly deactivates Mo_2C/CeO_2 through oxidation.

Deactivation is not only limited to Mo_2C/CeO_2, but is clearly seen for both Pt/CeO_2 and Mo_2C/γ-Al_2O_3 in Figure 2. To better understand the mechanism of rapid deactivation over Mo_2C/γ-Al_2O_3, reaction order measurements were performed for ethane. Clearly, as shown in the Supporting Information, the reaction order is negative with respect to ethane, meaning increasing concentrations of ethane decreases the catalytic activity. One explanation, obtained through DFT calculations, indicates the higher

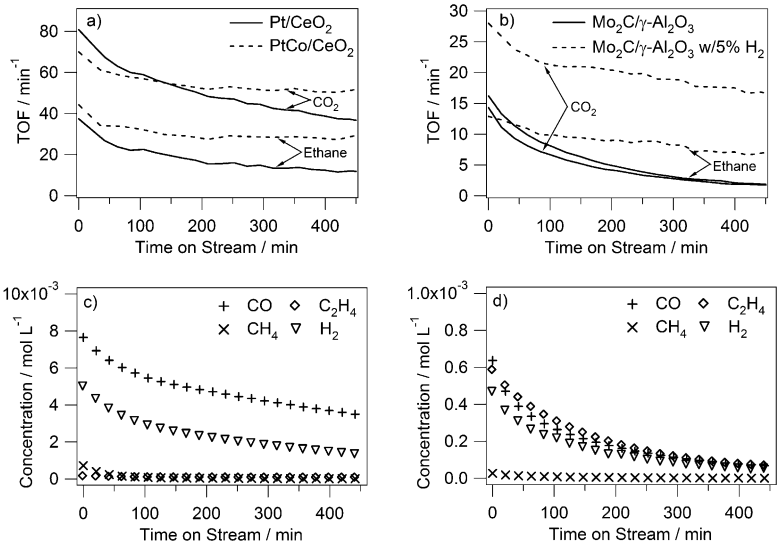

Figure 2. Turnover frequency (left column) and concentration of products (right column) for reactions of 10 mL min^{-1} ethane and CO_2 10 mL min^{-1} diluted in 20 mL min^{-1} He at 600 °C for a,c) Pt/CeO_2 and b,d) 8 %Mo_2C/γ-Al_2O_3 plotted versus time on stream. PtCo/CeO_2 and Mo_2C/γ-Al_2O_3 with 5 % H_2 (dashed) are included in (a) and (c), respectively as references.

Table 2: Summary of flow reactor data for CO_2 reduction by ethane experiments in 10 mL min^{-1} ethane and CO_2 diluted in 20 mL min^{-1} He at 600 °C. Values of conversion and selectivity calculated by averaging data points between 2–4.5 h on stream.

	Conversion [%]		Carbon Selectivity [%]			
Catalyst	CO_2	C_2H_6	CO	CH_4	C_2H_4	C_3+
Mo_2C	1.0	2.0	38.6	1.6	59.5	0.3
Mo_2C/γ-Al_2O_3	1.8	2.1	47.0	1.2	51.6	0.2
Mo_2C/CeO_2	0.3	0.1	88.1	2.1	9.8	0.0
Mo_2C/γ-Al_2O_3 w/H_2	8.8	3.8	73.4	0.7	25.7	0.2
Pt/CeO_2	28.0	9.5	97.8	0.8	1.4	0.0
$PtCo/CeO_2$	47.2	25.7	98.7	0.6	0.6	0.0
Pt/γ-Al_2O_3	12.4	1.7	95.2	0.7	4.1	0.0

binding energy of oxygen on Mo_2C destabilizes C–O bond formation and leads to ethylene as the primary product. The high selectivity towards ethylene, combined with the high binding energy on $Mo_2C(001)$ ($BE_{diff} = 1.14$ eV relative to Pt(111)), likely leads to coke formation through ethylene decomposition or polymerization,[25] partially explaining the deactivation and negative order.

To help mitigate the high deactivation over Mo_2C/γ-Al_2O_3, a small amount of H_2 (5 vol%) was added to the reaction feed to remove inactive oxide species to complete the catalytic cycle and restore some of the active carbidic phase, leading to higher activity (Figure 2c). This phenomenon has been seen in previous work over Mo_2C-based catalysts for CO_2 reduction by H_2.[18b] As shown in Table 2, the addition of H_2 improves the initial catalytic activity, but the CO selectivity increases while that of ethylene decreases. The increased selectivity toward CO is likely because the addition of H_2 promotes RWGS. Additionally, the Mo_2C/γ-Al_2O_3 catalyst can be regenerated through a post-reaction treatment cycle as shown in the Supporting Information.

To further understand the mechanism of deactivation over Mo_2C, in situ XANES measurements were performed over pure Mo_2C. Full details of the XANES experiments including spectra for pure Mo_2C in various reaction environments as well as the difference spectra (ΔXANES) can be found in Figure 4. The XANES measurements of Mo_2C show clear

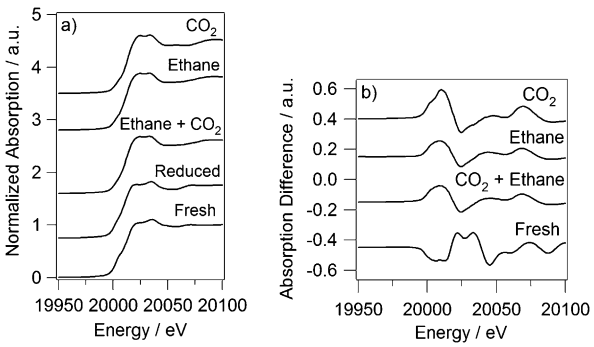

Figure 4. X-ray absorption near-edge structure measurements of Mo_2C in different gas environments, with a) raw spectra and b) ΔXANES subtracted from the "reduced sample". All spectra measured at room temperature after treatment at 450 °C for reduction and 600 °C for CO_2 and ethane environments.

Table 3: Results from linear combination fitting of Mo_2C XANES spectra.

Condition	Mo_2C	MoO_3	MoO_2
fresh	64.1	35.9	0
reduced	75.7	6.7	17.6
$C_2H_6 + CO_2$	23.5	0	76.5
C_2H_6	26.6	0	73.4
CO_2	0	9.6	90.4

changes in the oxidation state of Mo during all gas treatments, except for pure ethane. To quantify these changes, each Mo spectrum was fitted by a linear combination of Mo_2C, MoO_3, and MoO_2 standards, as described previously.[18a] The results of the linear combination fitting analysis are shown in Table 3.

By comparing the XANES results in Table 3, it is clear that treatment in H_2 removes a significant amount of the oxide species formed during passivation of the carbide during synthesis. Upon reaction of ethane and CO_2, Mo_2C is oxidized to a greater degree. Treatment in pure CO_2, however, completely oxidizes Mo_2C. Therefore, the adsorbed O from CO_2 is necessary to form an oxycarbide phase, which dehydrogenates ethane, but also likely contributes, at least partially, to the deactivation seen over Mo_2C-based catalysts.

In summary, Pt/CeO_2 and Mo_2C-based catalysts have been evaluated to catalytically control the products of CO_2 reduction by ethane to produce either synthesis gas or ethylene, respectively. Results of this study indicate that Pt/CeO_2 is a promising catalyst to produce synthesis gas, while Mo_2C/γ-Al_2O_3 preserves the C–C bond of ethane to produce ethylene, although the catalyst deactivates. These findings agree with DFT predictions that the Pt(111) surface preferentially forms synthesis gas, while $Mo_2C(001)$ leads to ethylene formation. Future studies should focus on designing materials that selectively produce ethylene with high stability and minimal deactivation.

Experimental Section

Spin-polarized DFT[26] calculations were performed using plane wave basis set Vienna Ab-Initio Simulation Package (VASP) code.[27] A plane wave cut-off energy of 400 eV and $3 \times 3 \times 1$ Monkhorst-Pack[28] grid were used for total energy calculations. Details of the DFT calculations are provided in the Supporting Information.

The synthesis procedures of Pt-based and Mo2C-based catalysts are provided in the Supporting Information. Reactions of ethane and CO_2 were carried out in a quartz reactor under atmospheric pressure. In each experiment, approximately 100 mg catalyst (60–80 mesh) was loaded into the flow reactor. Before the reaction, the catalyst was reduced under a 1:1 hydrogen and helium mixture (40 mL min^{-1} total flow) at 450 °C for 1 h. To start the reaction, the flow of CO_2 and ethane were each set at 10 mL min^{-1} with 20 mL min^{-1} of He as a diluent. For each experiment, the temperature was raised to 600 °C and the reaction was run for approximately 6 h.

X-ray absorption near-edge spectroscopy (XANES) measurements were used to confirm the oxidation state of Mo_2C under reaction conditions. Catalyst samples were diluted with boron nitride, pressed into a pellet, then grinded and sieved (100–150 mesh). The mass of catalyst and dilution were determined so the sample amount was two absorption lengths to maximize the signal-to-noise ratio of each sample. The XAFS spectra for Mo_2C was collected in a custom designed in situ glassy carbon cell,[32] using a 4-channel vortex fluorescence detector.

Acknowledgements

The work was carried out under contract number DE-SC0012704 with the U.S. Department of Energy, Office of Basic Energy Sciences. The DFT calculations were performed using computational resources at the Center for Functional Nanomaterials, a user facility at BNL, supported by the US Department of Energy and the National Energy Research Scientific Computing Center (NERSC) supported by the Office of Science of the U.S. Department of Energy under contract number DE-AC02-05CH11231.

Keywords: CO_2 · ethane · heterogeneous catalysis · surface chemistry · X-ray absorption

How to cite: *Angew. Chem. Int. Ed.* **2015**, *54*, 15501 – 15505
Angew. Chem. **2015**, *127*, 15721 – 15725

[1] N. Mimura, I. Takahara, M. Inaba, M. Okamoto, K. Murata, *Catal. Commun.* **2002**, *3*, 257 – 262.
[2] M. M. Bhasin, J. H. McCain, B. V. Vora, T. Imai, P. R. Pujadó, *Appl. Catal. A* **2001**, *221*, 397 – 419.
[3] V. Choudhary, K. Mondal, S. R. Mulla, *J. Chem. Sci.* **2006**, *118*, 261 – 267.
[4] a) T. R. Knutson, R. E. Tuleya, *J. Clim.* **2004**, *17*, 3477 – 3495; b) J. Hansen, M. Sato, R. Ruedy, K. Lo, D. W. Lea, M. Medina-Elizade, *Proc. Natl. Acad. Sci. USA* **2006**, *103*, 14288 – 14293.
[5] T. Osaki, T. Mori, *React. Kinet. Catal. Lett.* **2006**, *89*, 333 – 339.
[6] M. S. Fan, A. Z. Abdullah, S. Bhatia, *ChemCatChem* **2009**, *1*, 192 – 208.
[7] X. D. Xu, J. A. Moulijn, *Energ. Fuego At. Energ. Fuel* **1996**, *10*, 305 – 325.
[8] C. A. Gärtner, A. C. van Veen, J. A. Lercher, *ChemCatChem* **2013**, *5*, 3196 – 3217.
[9] a) M. D. Argyle, K. D. Chen, A. T. Bell, E. Iglesia, *J. Catal.* **2002**, *208*, 139 – 149; b) H. H. Kung, in *Adv. in Catal.*, *Vol. 40* (Eds.: D. D. Eley, H. Pines, W. O. Haag), Elsevier Academic Press, San Diego, **1994**, pp. 1 – 38.
[10] a) E. Heracleous, A. A. Lemonidou, *J. Catal.* **2006**, *237*, 175 – 189; b) G. Grubert, E. Kondratenko, S. Kolf, M. Baerns, P. van Geem, R. Parton, *Catal. Today* **2003**, *81*, 337 – 345.
[11] N. Mimura, M. Okamoto, H. Yamashita, S. T. Oyama, K. Murata, *J. Phys. Chem. B* **2006**, *110*, 21764 – 21770.
[12] L. Jin, J. Reutenauer, N. Opembe, M. Lai, D. J. Martenak, S. Han, S. L. Suib, *ChemCatChem* **2009**, *1*, 441 – 444.
[13] S. Wang, K. Murata, T. Hayakawa, S. Hamakawa, K. Suzuki, *Appl. Catal. A* **2000**, *196*, 1 – 8.
[14] S. Deng, H. Li, S. Li, Y. Zhang, *J. Mol. Catal. A* **2007**, *268*, 169 – 175.
[15] a) K. Nakagawa, M. Okamura, N. Ikenaga, T. Suzuki, T. Kobayashi, *Chem. Commun.* **1998**, 1025 – 1026; b) T. Baidya, N. van Vegten, A. Baiker, *Top. Catal.* **2011**, *54*, 881 – 887.
[16] F. Solymosi, R. Németh, *Catal. Lett.* **1999**, *62*, 197 – 200.
[17] M. D. Porosoff, J. G. Chen, *J. Catal.* **2013**, *301*, 30 – 37.
[18] a) M. D. Porosoff, X. Yang, J. A. Boscoboinik, J. G. Chen, *Angew. Chem. Int. Ed.* **2014**, *53*, 6705 – 6709; *Angew. Chem.* **2014**, *126*, 6823 – 6827; b) M. D. Porosoff, S. Kattel, W. Li, P. Liu, J. G. Chen, *Chem. Commun.* **2015**, *51*, 6988 – 6991.
[19] Z. Duan, G. Wang, *Phys. Chem. Chem. Phys.* **2011**, *13*, 20178 – 20187.
[20] H. Ren, W. Yu, M. Salciccioli, Y. Chen, Y. Huang, K. Xiong, D. G. Vlachos, J. G. Chen, *ChemSusChem* **2013**, *6*, 798 – 801.
[21] a) W. Yu, M. Salciccioli, K. Xiong, M. A. Barteau, D. G. Vlachos, J. G. Chen, *ACS Catal.* **2014**, *4*, 1409 – 1418; b) S. Posada-Pérez, F. Vines, P. J. Ramirez, A. B. Vidal, J. A. Rodriguez, F. Illas, *Phys. Chem. Chem. Phys.* **2014**, *16*, 14912 – 14921.
[22] A. Bruix, J. A. Rodriguez, P. J. Ramírez, S. D. Senanayake, J. Evans, J. B. Park, D. Stacchiola, P. Liu, J. Hrbek, F. Illas, *J. Am. Chem. Soc.* **2012**, *134*, 8968 – 8974.
[23] a) T. Staudt, Y. Lykhach, N. Tsud, T. Skála, K. C. Prince, V. Matolín, J. Libuda, *J. Catal.* **2010**, *275*, 181 – 185; b) L. Appel, J. Eon, M. Schmal, *Catal. Lett.* **1998**, *56*, 199 – 202.
[24] a) P. Concepción, A. Galli, J. M. L. Nieto, A. Dejoz, M. I. Vazquez, *Top. Catal.* **1996**, *3*, 451 – 460; b) J. Ogonowski, E. Skrzyńska, *React. Kinet. Catal. Lett.* **2006**, *88*, 293 – 300.
[25] R. J. Zou, Q. K. Lou, S. H. Mo, S. B. Feng, *Ind. Eng. Chem. Res.* **1993**, *32*, 843 – 847.
[26] a) P. Hohenberg, W. Kohn, *Phys. Rev.* **1964**, *136*, B864 – B871; b) W. Kohn, L. J. Sham, *Phys. Rev.* **1965**, *140*, A1133 – A1138.
[27] a) G. Kresse, J. Furthmüller, *Comput. Mater. Sci.* **1996**, *6*, 15 – 50; b) G. Kresse, J. Hafner, *Phys. Rev. B* **1993**, *48*, 13115 – 13118.
[28] H. J. Monkhorst, J. D. Pack, *Phys. Rev. B* **1976**, *13*, 5188 – 5192.
[29] a) G. Kresse, D. Joubert, *Phys. Rev. B* **1999**, *59*, 1758 – 1775; b) P. E. Blöchl, *Phys. Rev. B* **1994**, *50*, 17953 – 17979.
[30] J. P. Perdew, Y. Wang, *Phys. Rev. B* **1992**, *45*, 13244 – 13249.
[31] R. Hou, K. Chang, J. Chen, T. Wang, *Top. Catal.* **2015**, *58*, 240 – 246.
[32] A. M. Karim, C. Howard, B. Roberts, L. Kovarik, L. Zhang, D. L. King, Y. Wang, *ACS Catal.* **2012**, *2*, 2387 – 2394.

Received: August 31, 2015
Revised: October 6, 2015
Published online: November 10, 2015

